DOI: 10.18721/JPM.14307
UDC 532.517

THERMAL MANIKIN SHAPE INFLUENCE ON AIRFLOW AND HEAT TRANSFER IN THE MODEL ROOM WITH DISPLACEMENT VENTILATION

E.D. Stepasheva, M.A. Zasimova, N.G. Ivanov

Peter the Great St. Petersburg Polytechnic University,
St. Petersburg, Russian Federation

The paper presents the results of numerical modeling of turbulent flow and heat transfer in the model room with displacement ventilation. The goal of the study is to assess the shape influence of the thermal manikin placed in the room on the computed airflow structure. Three manikin shapes have been considered: a detailed one (close to a human shape) and ones simplified partially and completely. The problem formulation was close to the test conditions of P.V. Nielsen et al. (2003). The RANS approach based on the standard k-ε turbulence model was applied. The study revealed solution sensitivity to the dimension and topology of the mesh used, as well as the solution dependence on the uncertainty of the inlet velocity distribution. The calculated results were shown to agree generally with the experimental data. The simplification of the manikin shape had a significant impact on the local parameter prediction accuracy.

Keywords: ventilation, thermal manikin, turbulent airflow and heat transfer, natural convection

Citation: Stepasheva E.D., Zasimova M.A., Ivanov N.G., Thermal manikin shape influence on airflow and heat transfer in the model room with displacement ventilation, St. Petersburg Polytechnical State University Journal. Physics and Mathematics. 14 (3) (2021) 90–106. DOI: 10.18721/JPM.14307

ВЛИЯНИЕ ФОРМЫ ТЕПЛОВОГО МАНЕКЕНА НА ТЕЧЕНИЕ И ТЕПЛООБМЕН В МОДЕЛЬНОМ ПОМЕЩЕНИИ С ВЫТЕСНЯЮЩЕЙ ВЕНТИЛЯЦИЕЙ

Е.Д. Степашева, М.А. Засимова, Н.Г. Иванов

Санкт-Петербургский политехнический университет Петра Великого,
Санкт-Петербург, Российская Федерация

В работе представлены результаты численного моделирования турбулентного течения и теплообмена в модельном помещении с вытесняющей вентиляцией, в котором размещен нагретый тепловой манекен. Цель работы – оценить влияние формы манекена на структуру течения воздуха, предсказываемую расчетами. Рассмотрены три формы манекена: детальная (приближена к форме человека), а также частично и полностью упрощенные. Постановка задачи приближена к условиям тестового эксперимента P.V. Nielsen и др. (2003). Моделирование турбулентности осуществлялось с помощью RANS-подхода с привлечением стандартной k-ε модели турбулентности в сочетании с методикой разрешения пристенной области. В результате исследования выявлена степень чувствительности решения к размерности и топологии используемой сетки, а также влияние на решение неопределенности входного распределения скорости. Показано, что расчетные результаты в целом согласуются с данными эксперимента; упрощение формы манекена оказывает существенное влияние на точность предсказания локальных параметров.

Ключевые слова: вентиляция, тепловой манекен, турбулентное течение и теплообмен, естественная конвекция

Ссылка при цитировании: Степашева Е.Д., Засимова М.А., Иванов Н.Г. Влияние формы теплового манекена на течение и теплообмен в модельном помещении с вытесняющей вентиляцией // Научно-технические ведомости СПбГПУ. Физико-математические науки. 2021. Т. 14. № 3. С. 90–106. DOI: 10.18721/JPM.14307

Introduction

Ventilation systems must provide thermally comfortable characteristics, maintaining a microclimate that is suitable for humans in ventilated rooms. The following characteristics are commonly used to assess the thermal comfort in practice [1, 2]:

draught rating (DR),

predicted mean vote (PMV),

predicted percentage of dissatisfied (PPD),

percentage dissatisfied with the vertical air temperature difference (Percentage Dissatisfied).

When it comes to ventilation systems that have already been put into operation, these characteristics are assessed from interviews with people in the room using a special technique. The characteristics of thermal comfort can also be estimated based on initial data on airflow: local and/or integral velocities, velocity fluctuations and (for non-isothermal problems) temperatures, using the empirical relations listed in the standards.

Formulating and solving applied ventilation problems generates a large number of parameters that are difficult (and often impossible) to define unambiguously. These are, in particular, the following parameters:

person's position in the room and its variation over time,

shape of the person's body (individual geometry, positions of individual body parts),

individual heat transfer characteristics (local and integral),

thermal insulation of the clothing, etc.

While the above parameters significantly affect the flow and heat transfer characteristics, and, as a consequence, the thermal comfort characteristics, all of them can be fully taken into account only in some simple cases. It is often convenient, and sometimes in fact necessary to simplify the problem statement for both physical experiment and computational fluid dynamics (CFD). This decision needs to be substantiated in each case.

Physical experiments considering the characteristics of thermal comfort in a room with people widely employ thermal manikins simulating humans, including heat release and breathing. Computational studies of ventilation flow also frequently involve 'virtual' thermal manikins (see, for example, [3 – 5]). Ref. [6] thoroughly reviews the state of the art in numerical simulation of airfllow and heat transfer near a thermal manikin [6].

Numerical simulation, especially in fundamental studies, is best performed with a simplified shape of the thermal manikin rather than the detailed geometry of the human body, since this allows controlling the conditions of the computational experiment more precisely (for example, the quality of the mesh near a solid surface). Example computations are given in [7, 8] for flow and heat transfer in the vicinity of a thermal manikin with a simplified shape; the results were obtained based on an eddy-resolving method for Large Eddy Simulation. However, standard thermal manikins are typically used in modern physical experiments: they have a detailed shape, so additional comprehensive studies are required to directly compare the computational results obtained for a simplified manikin with the experimental data.

The degree to which the shape of the thermal manikin influences the structure of the flow in the room was previously assessed for various configurations both in experimental studies [9, 10] and based

on CFD [8, 11, 12]. Conclusions on the effect that the shape of the manikin has on the local characteristics of the flow were drawn in [8 – 12] for particular cases in each of the given problems.

Experimental data have been accumulated in the literature for two test configurations corresponding to two types of ventilation: mixing [10, 13] and displacement [13]. In the first case, the air supplied through the inlets is mixed well in the room, for example, due to global circulation. With displacement ventilation (second case), fresh air is supplied to the bottom of the room, and the exhaust openings are located near the ceiling, which minimizes global mixing. Experiments in [10, 13] considered a test room containing a heated manikin with controlled heat release from the skin surface. The experiments measuring the velocity and temperature fields, carried out in several sections of the room, were interpreted by the authors as benchmarks. The results of experimental measurements, well documented and posted by the authors as a database at http://www.cfd-benchmarks.com/, have been repeatedly used to validate the computational data [8, 14 – 16]: Refs. [8, 14] present the computational results for a room with displacement ventilation, and Refs. [15, 16] discuss a room with mixing ventilation.

This paper provides the results for numerical study of flow and heat transfer near a thermal manikin for the test conditions with displacement ventilation [13].

Our goal was to assess the degree of sensitivity of the flow structure in the room to changes in the geometric shape of the thermal manikin.

The computations were carried out for three shapes of the manikin: detailed (close to the shape of the human body and largely corresponding to the one adopted in the experiment), partially simplified (consisting of parallelepiped blocks), and completely simplified (one solid parallelepiped). Turbulence was simulated using the RANS approach with the standard k-ε turbulence model, which is the most widespread in studies of jet flows.

Problem statement

Geometric model. We consider a ventilated room (Fig. 1,*a*); its height, width and length (in meters) are $H = 2.7$, $W = 3.0$ and $L = 3.5$, respectively. The coordinate system used is shown on the schematic of the room, the origin of the coordinate system is located in its bottom left corner. One of the sidewalls has a rectangular inlet opening near the floor, with the height $h_{in} = 0.2$ m and the width $w_{in} = 0.4$ m. The equivalent inlet diameter $D_e = (4h_{in}w_{in}/\pi)^{1/2} = 0.3$ m. The outlet has a square shape $h_{out} = w_{out} = 0.3$ m and is located on the opposite sidewall near the ceiling of the room. The inlet and outlet are centered along the z coordinate.

A thermal manikin is located in the center of the room; its surface is h = 0.05 m above the floor. We considered three shapes of the thermal manikin: parallelepiped, block and detailed (see also Table 1). The manikin is in an upright position, facing the inlet. The simplest of the given shapes is a parallelepiped (Fig. 1,*b*) with the following dimensions: height $h_m = 1.7$ m, width $w_m = 0.4$ m and thickness $l_m = 0.1$ m. The surface area of the manikin is $S_m = 1.78$ m^2.

The geometric parameters of the block shape (Fig. 1,*c*) are the same as in [8]. The block-shaped manikin is made up of parallelepipeds, which taken together imitate the real shape of the human body to some degree. The manikin also has the following separate parts: head, two arms, torso and two legs (Table 2). The surface area of the manikin is $S_m = 1.48$ m^2 (see Table 1).

The detailed shape of the manikin (Fig. 1,*d*) is close to that used in the experiment. The manikin geometry was produced with the MakeHuman software (official website: *makehumancommunity.org*).

Note that the area of the thermal manikin used in the experimental study [13] is $S_m = 1.47$ m^2. This value is 7% less than for the detailed shape of the manikin discussed in this paper. The reason for this is that the shape of the manikin used in [13] cannot be reproduced completely because the geometry was described insufficiently, even though the measurement results were fairly well documented. While the experiments in [13] were carried out for both the sitting and standing positions of the manikin

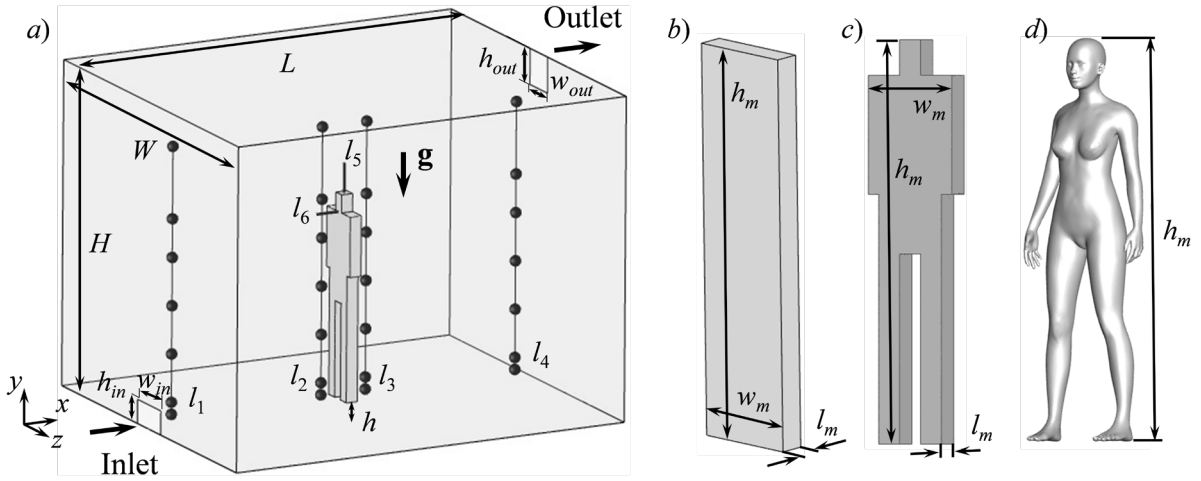

Fig. 1. Schematic of the room (*a*) and different shapes of the manikin: parallelepiped (*b*), block (*c*), detailed (*d*).
Inlet and outlet of the airflow, and geometric parameters are shown;
lines $l_1 - l_6$ mark the positions of the sections for which experimental data are available

Table 1

Computational configurations accounting for manikin shape and external factors

Manikin shape (S_m, m^2)	q_w, W/m^2	Computational grid, mln	Element type	y_p, mm	$\langle y^+ \rangle$
Parallelepiped (1.78)	21	0.79	Hexagonal	1.0	1.12
		0.97		0.5	0.58
		0.24	Polyhedral	5.0	4.74
		1.16		1.0	1.05
Block (1.48)	26	1.04		1.0	1.05
Detailed (1.57)	24	1.62		1.0	1.02

N o t a t i o n s: S_m is the surface area, q_w is the specific heat flux, y_p is the height of the first near-wall cell at the surface of the manikin, $\langle y^+ \rangle$ is the averaged dimensionless distance from the manikin surface to the center of the first near-wall cell.

(the latter is also considered in our study), the geometry on http://www.cfd-benchmarks.com/ is only given for the sitting position.

Lines $l_1 - l_6$ shown in Fig. 1,a demonstrate the positions of the sections for which experimental data are available in [13]. All lines are located in the central plane of the room: for $z = 1.5$ m. Lines $l_1 - l_4$ are located at distances 0.20, 1.55, 1.95 and 3.30 meters from the inlet. The symbols in the figure mark the positions of the points where the velocity magnitude (measured with an ultrasonic anemometer) and temperature (measured with a thermocouple) were captured along the lines. The database contains velocities obtained by Particle Image Velocimetry (PIV) for lines l_5, l_6 (their positions are $x = 1.75$ m and $y = 1.60$ m).

Physical parameters of the environment and boundary conditions. The physical properties of the air were taken constant and corresponded to a temperature of 22 °C:

density $\rho = 1.194$ kg/m^3,

Table 2

Geometrical parameters for three manikin shapes

Parameter of manikin/part	Size for shape, m		
	parallelepiped	block	detailed
Height h_m	1.70	1.70	1.70
Maximum width w_m	0.40	0.40	0.59
Thickness l_m	0.10	0.30	0.30
Head	–	0.15×0.10	MakeHuman software used
Body		0.75×0.30	
Arm (two)		0.50×0.05	
Leg (two)		0.80×0.10	
Distance between legs		0.10	

N o t e. The sizes of the manikin parts for the block shape are given in the *yz* plane.

dynamic viscosity $\mu = 1.789 \cdot 10^{-5}$ kg/(m·s),
specific heat $C_p = 1006$ J/(kg·K),
thermal conductivity $\lambda = 0.024$ W/(m·K).
The Prandtl number with such parameters equals $\mathrm{Pr} = \mu C_p/\lambda = 0.69$.

According to documentation for the experiment in [13], it is preferable to set a uniform velocity profile $V_{in} = 0.2$ m/s at the inlet to the room. This condition was reproduced in the main series of computations, which corresponds to a volumetric flow rate of 57.6 m^3/h. The Reynolds number calculated from the equivalent diameter and inlet velocity is in this case $\mathrm{Re} = \rho D_e V_{in}/\mu = 4300$.

In addition to recommendations, the appendix to the experimental data in [13] on the website contains a table (in Excel format) of measured magnitudes of the inlet velocity. According to these data, the mean flow velocity at the inlet is 0.181 m/s. Additional computations were performed for the configuration with a block-shaped manikin, with a uniform velocity profile given at the inlet $V_{in} = 0.181$ m/s (the corresponding flow rate was 52.1 m^3/h). Another series of computations were performed for a non-uniform velocity profile at the inlet, obtained from the solution to the problem of flow in a channel with the corresponding section, where the bulk velocity was $V_{in} = 0.181$ m/s.

Constant pressure boundary conditions were imposed at the inlet to the computational domain. The no-slip condition was imposed on the walls of the ventilated room and on the surface of the manikin.

The following thermal boundary conditions were imposed in accordance with the experimental conditions in [13]:
inlet temperature was constant and equal to $T_{in} = 22$ °C,
the walls of the room were adiabatic.

The integral heat removal from the manikin surface was taken equal to $Q_w = 38$ W for all geometric configurations, which corresponds to 50% of the value adopted in the standards for a person standing still. If the computations for the thermal manikin do not account for the radiative heat transfer (as is the case in this study), a customary technique is to reduce the typical heat release for a person by approximately two times. A constant value of the specific heat flux was given on the surface of the manikin, defined as $q_w = Q_w/S_m$. The values of the specific heat flux used for different geometric shapes of the manikin are given in Table 1.

Mathematical and computational models. Turbulence was simulated by the RANS approach (solving the Reynolds-averaged Navier – Stokes equations); for more details see, for example, mono-

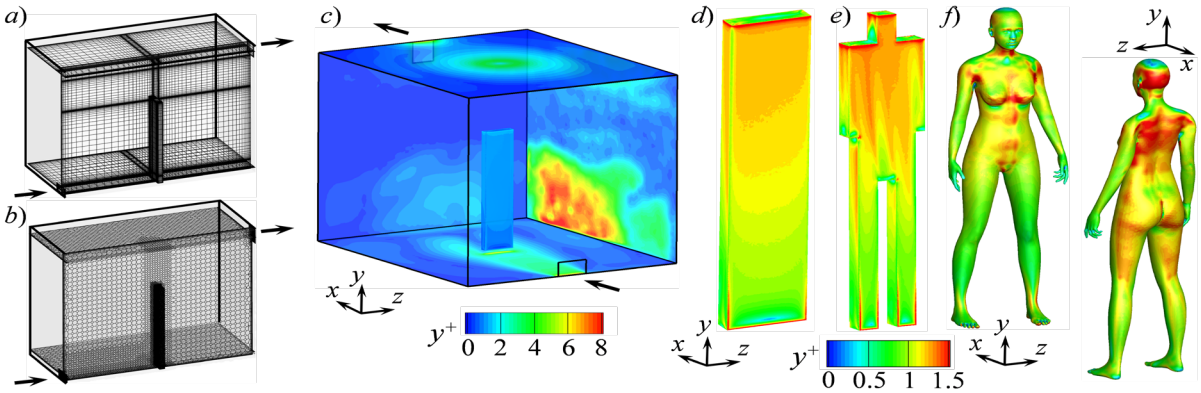

Fig. 2. General view of computational meshes with hexagonal elements (0.79 million) (*a*) and polyhedral elements (1.16 million) (*b*) for parallelepiped-shaped manikin; distribution of y^+ along room wall surfaces (mesh of 1.16 million cells) (*c*) and along surfaces of three shapes of manikins: parallelepiped (*d*), block (*e*) and detailed (*f*)

graph [17]. The equations are closed by the standard semi-empirical *k*-ε turbulence model [18] combined with the Enhanced Wall Treatment technique for resolving the near-wall region. The following turbulence characteristics were adopted in the computations at the inlet to the room:

turbulence intensity $I = 30\%$,

ratio of turbulent to molecular viscosity $\mu_t/\mu = 44$.

The buoyancy force was taken into account using the Boussinesq approximation. The gravitational acceleration vector **g**, whose magnitude equals $g = 9.81$ m/s^2, is directed vertically down towards the floor of the room (see Fig. 1,*a*). The volumetric thermal expansion coefficient was given as $\beta = = 3.39 \cdot 10^{-3}$ K^{-1}.

The computations used quasi-structured meshes with hexagonal elements, constructed in the ICEM CFD 2019 R3 mesh generator, as well as unstructured meshes with polyhedral elements obtained in ANSYS Fluent by transforming computational meshes with tetrahedral elements built in ICEM CFD. The sizes and some other characteristics of the computational meshes used in the study are given in Table 1. The appearance of meshes with hexagonal and polyhedral elements is shown in Fig. 2,*a*,*b*. The meshes are clustered towards the walls of the computational domain, as well as towards the surface of the manikin.

Meshes with hexagonal elements were used for the simplest form of a manikin, i.e., a parallelepiped. Two types of mesh with hexagonal elements were constructed, with varying height y_p of the first near-wall cell at the surface of the manikin (see Table 1): this dimension was 1 mm for the first type, the total size of the mesh was 790,000 (82 × 109 × 90) cells, and 0.5 mm for the second type (half as much), while the total mesh size was 970,000 (98 × 111 × 92) cells. The value of the dimensionless distance y^+ from the manikin surface to the center of the first near-wall cell (see Fig. 2,*a*), is, on average, 1.12 and 0.58 for the types, respectively.

Two meshes consisting of polyhedral elements were also constructed for the parallelepiped-shaped manikin. A more economical mesh containing 240,000 elements in total had five prismatic layers without clustering near the walls perpendicular to the axes *x* and *y* or near the manikin surface; the transverse size of the cells in the layers was $y_p = 5$ mm. The rest of the area, that is, the inner part of the room, was divided into identical polyhedral cells with the characteristic size of 10 cm. This mesh topology is often used in engineering practice because it is easy to generate. The second polyhedral mesh, with a total of 1.16 million elements, was clustered around the near-wall jet, as well as in the region above the manikin (see Fig. 2,*b*). The characteristic size of polyhedral elements was 5 cm

in the refined regions, and 10 cm in the rest of the domain. Ten prismatic layers were given near the manikin surface with a clustering coefficient of 1.1 to the surface of the manikin; the height of the first near-wall layer is y_p = 1 mm. The distribution of y^+ for this configuration of the computational mesh is shown in Fig. 2,*c*,*d*. The value of y^+ does not exceed 10 on the walls of the room, averaging to 1.05 over the manikin surface.

The computational mesh for the block and detailed shapes of the manikin consisted of prismatic layers and polyhedral cells with characteristics similar to the polyhedral mesh with clustering for the parallelepiped-shaped manikin. The distribution of y^+ on the surface of the manikins for these cases is shown in Fig. 2,*d*,*f*. The values of y^+ on the surface of the manikin also amounted to about 1 on average (see Table 1).

All computations were performed in the ANSYS Fluent 2019 R3 CFD package. The equations were approximated with second-order precision. The SIMPLE method was chosen to organize the iterative process. The resources of the SPbPU Fluid Dynamics Research Laboratory cluster (maximum of 24 cores) were used.

Computational results and discussion

Mesh sensitivity analysis. Fig. 3 shows the velocity profiles in six sections of the room $l_1 - l_6$, obtained in computations for the parallelepiped-shaped manikin with meshes of different dimensions and topology (see Table 1).

The graphs for the sections l_1 and l_2 (Fig. 3,*a*,*b*) show a zone where a near-wall inlet jet propagates (at $y < 0.6$ m). The jet intensity decreases downstream; the velocity magnitude changes from the inlet value, equal to 0.20 m/s, to the corresponding value in front of the manikin surface, equal to 0.15 m/s. The velocity profiles shown in the sections l_1 and l_2 vary little as the computational

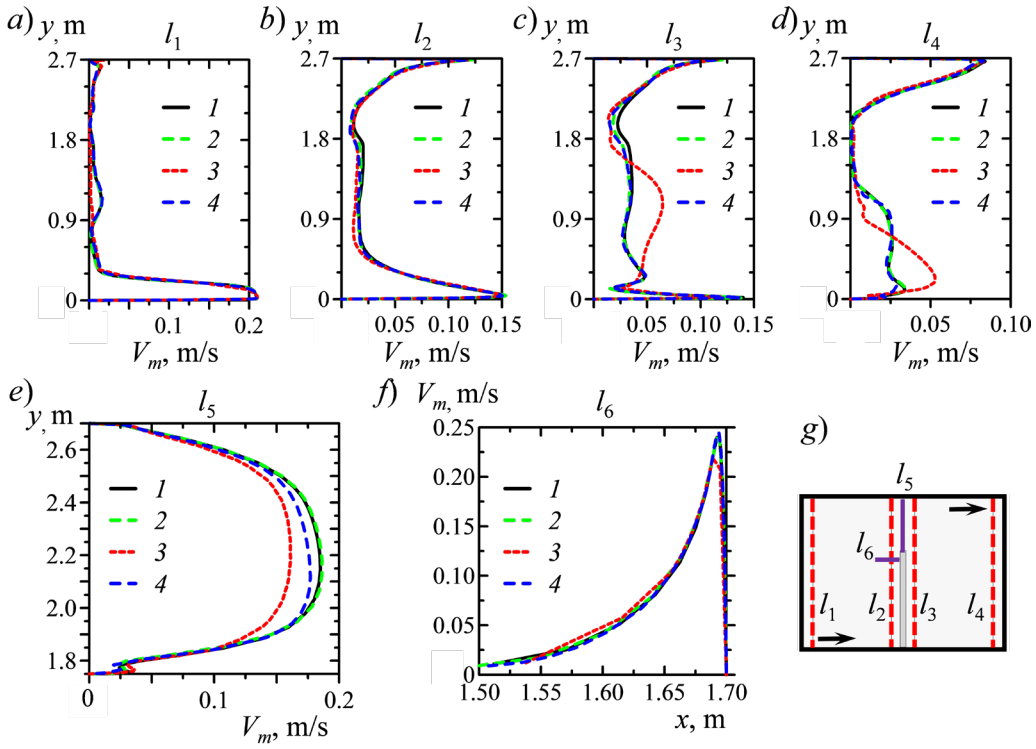

Fig. 3. Velocity profiles (*a* – *f*) plotted along lines $l_1 - l_6$ (see Fig. 1) obtained in solutions with meshes of different dimensions: 0.79 (*1*), 0.97 (*2*), 0.24 (*3*) and 1.16 (*4*); *g* shows the layout of the sections

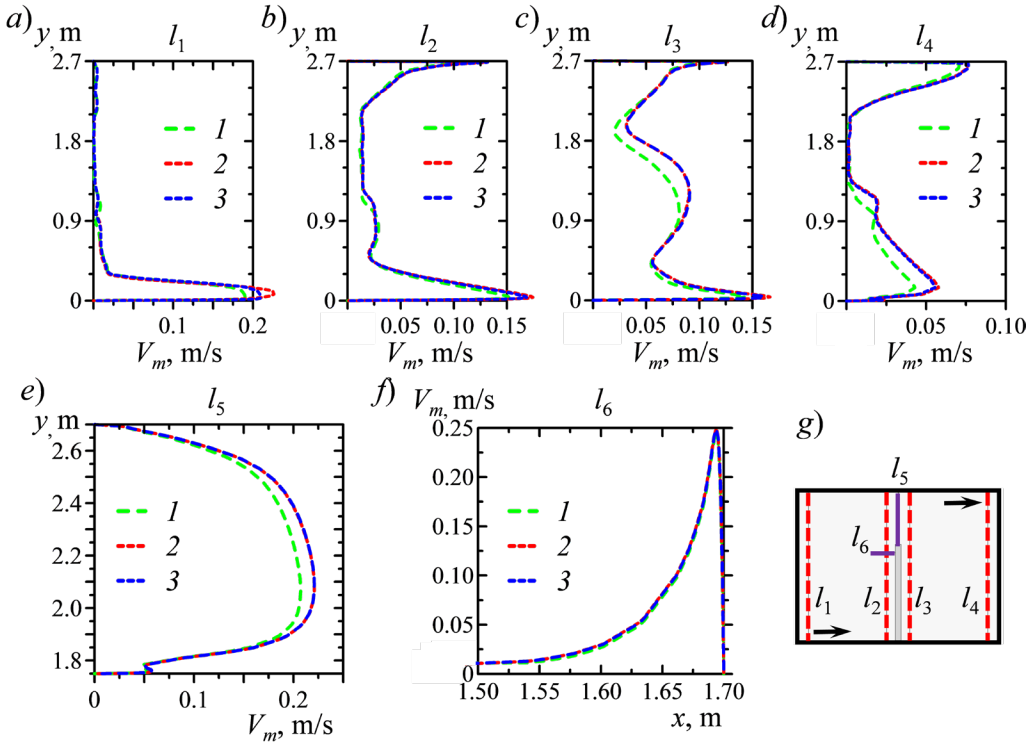

Fig. 4. Velocity profiles ($a - f$) plotted along the lines $l_1 - l_6$ (see Fig. 1) obtained for different inlet velocity distributions: uniform, equal to 0.181 m/s (*1*); non-uniform profile with a bulk velocity of 0.181 m/s (*2*); uniform, equal to 0.200 m/s (*3*); *g* is the layout of the sections

mesh is altered, although the solution on the coarsest mesh *3* is apparently somewhat different from the others. The obtained solution is considerably sensitive to the computational mesh used, which is manifested in the wake behind the manikin, as evident from the velocity graphs in the sections l_3 and l_4 for the bottom of the room at $y < 1.8$ m (Fig. 3,*c*,*d*). The flow here is characterized by reduced velocities. The solution obtained with a mesh with fewer elements (240,000) is markedly different from the solutions obtained on more refined meshes.

Velocity graphs plotted in sections l_5 and l_6 (Fig. 3,*e*,*f*), as well as in the top of the room in sections l_2 and l_3 at $y \geq 1.8$ m (Fig. 3,*b*,*c*) illustrate free-convection flow evolving near the surface of the thermal manikin and in the thermal plume above it due to buoyancy. A free-convection boundary layer emerges near the manikin surface, where the characteristic velocities in the upper part of the manikin reach 0.25 m/s (Fig. 3,*f*). A weak dependence of the solution on the dimension of the mesh used in the computations is observed in this region. The solution is somewhat sensitive to the mesh near the thermal plume generated above the manikin. Analyzing the data for the velocity distribution shown in Fig. 3,*e*, we can conclude that the velocities in this region, computed on a mesh with 240,000, are 15% lower than for other meshes. Importantly, the temperature fields obtained in the computations with all meshes considered practically coincide.

Notice that the three solutions obtained on two hexagonal meshes and on a mesh with clustered polyhedral elements are nearly the same. This means that the solution obtained on a mesh with clustered polyhedral cells can be considered weakly dependent on the mesh. Because of this, meshes with similar topology and dimensions were used for the configurations with the block-shaped and detailed manikins.

Sensitivity of the solution to the inlet velocity distribution. This sensitivity was studied for the configuration with the block-shaped manikin. Three inlet distributions were given:

uniform velocity distribution $V_{in} = 0.2$ m/s, recommended in [13];

uniform velocity distribution $V_{in} = 0.181$ m/s (mean value according to the experimental data given in the appendix to [13]);

velocity distribution obtained by additionally computing the flow in a rectangular channel $h_{in} \times w_{in}$ with a length of $15h_{in}$, with the bulk velocity of 0.181 m/s.

Fig. 4 shows the velocity profiles in the sections $l_1 - l_6$, obtained in solutions with different inlet velocity distributions. The graph in Fig. 4,*a* for the section l_1 shows the differences in the solutions obtained: the maximum velocities in the region of the near-wall jet (at $y < 0.6$ m) are in the range of 0.19 – 0.23 m/s. The velocity profiles in the remaining sections in Fig. 4 ($l_2 - l_6$), away from the inlet, only differ slightly: there are some differences in the region with reduced velocities in the sections l_3 and l_4, as well as in the thermal plume zone above the manikin (section l_5). The data presented in Fig. 4 indicate that the obtained solution changes little within the given range of inlet flow rates. A uniform distribution of $V_{in} = 0.2$ m/s was used in the main series of computations.

Effect of manikin shape on flow and heat transfer

Description of the flow structure. Fig. 5 illustrates the flow structure in a ventilated room, showing streamlines colored by velocity magnitude (Fig. 5,*a*,*c*,*d*), as well as the velocity fields in several sections of the room (Fig. 5,*b*,*e*,*f*), constructed for three manikin shapes.

The solutions obtained allow distinguishing two regions in the flow. The first one is where the near-wall jet propagates in the bottom of the room, interacting with the manikin. The second is the region with buoyancy-induced free-convection upward airflow. This flow evolves near and above the surface of the heated manikin, producing a thermal plume initiating secondary flow in the top of the room. Both regions have comparable velocities and interact little with each other.

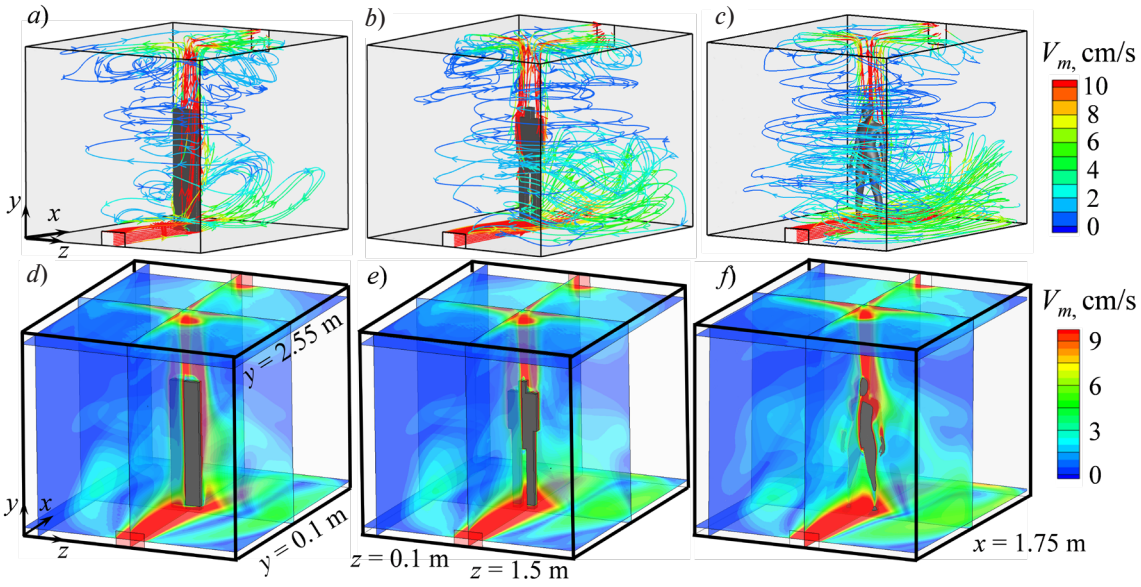

Fig. 5. Streamlines ($a - c$) colored by velocity magnitude; velocity magnitude fields ($d - f$) in several sections of the room, obtained in computations with three manikin shapes: parallelepiped (*a*, *d*), block (*b*, *e*), detailed (*c*,*f*)

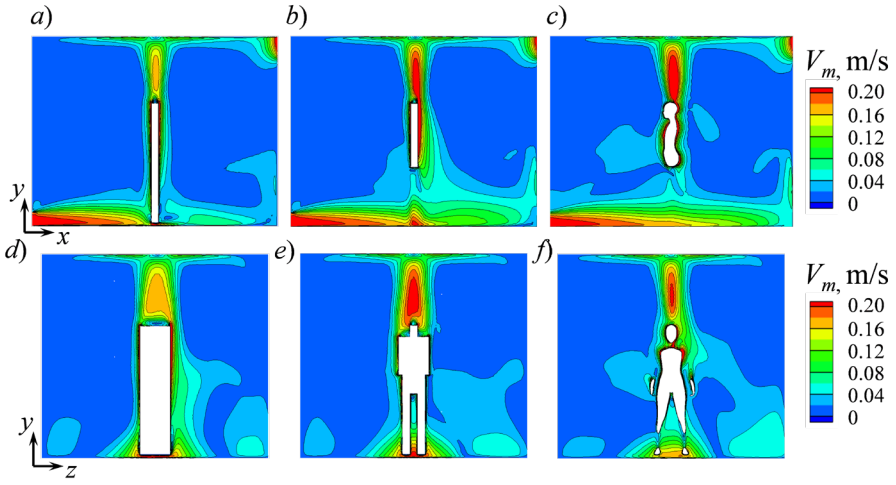

Fig. 6. Velocity magnitude distributions in two sections of the room: $z = 1.50$ m ($a - c$) and $x = 1.75$ m ($d - f$) computed for three manikin shapes: parallelepiped (a, d), block (b, e), detailed (c, f)

Fig. 6 shows the velocity fields in two central sections of the room: $z = 1.50$ m and $x = 1.75$ m (the velocity fields in Fig. 5,*d*,*e*,*f* are shown in isometric projection for the same sections). The flow structure obtained in the computations for all shapes of the manikin was asymmetric relative to the central plane $z = 1.5$ m. The near-wall jet spreads from the inlet along the floor, interacts with the manikin, attenuates and collides with the sidewall opposite from the inlet. When the jet interacts with the wall, the flow rate is distributed unevenly, and, after turning around, the backflow along one of the bottom corners of the room appears to be more intense than along the opposite corner. This is evident from the local maximum velocities in the bottom right part of the room (Fig. 6,*d*,*e*,*f*). Nota-bly, an asymmetric solution was obtained for both topologies of the computational mesh used for the parallelepiped-shaped manikin.

Figs. 5 and 6 show the results for the solution with the jet attaching to the right side wall, which is not unique, apparently. Two steady solutions (converging by residuals) were obtained for the parallelepiped-shaped manikin, with the jet attaching to the opposite side walls of the ventilated room. It was found for both computational mesh topologies that the solution was not unique.

The data obtained show that the global flow structure evolving in the room changes little with the change in the manikin shape. However, the local flow characteristics change depending on the manikin shape. For example, differences in the velocity fields are observed in the jet zone where the jet interacts with the manikin (Fig. 6). Differences in the characteristic velocities in the thermal plume above the manikin are observed in the region with free-convection flow. The maximum velocities in the thermal plume were 0.180 m/s for the parallelepiped-shaped manikin, 0.230 m/s for the block shape, 0.255 m/s for the detailed one. Thus, the intensity of free-convection flow is higher for manikins with detailed and block shapes than for the parallelepiped-shaped manikin.

Comparison of computational and experimental data. The results of numerical simulation were compared with the experimental data from [13] (Fig. 7). Fig. 7,*a* schematically shows the locations of sections I and II where PIV measurements were carried out in [13]. Both sections are in the center of the room ($z = 1.5$ m): section I above the manikin, and section II in front of it, near the face. Fig. 7,*b*,*c* shows the distribution of the velocity magnitude near the manikin surface in sections I and II based on experimental data from [13]. The velocity magnitude is constructed by two components V_x and V_y, however, the position of the coordinate axes x', y' is not described exactly

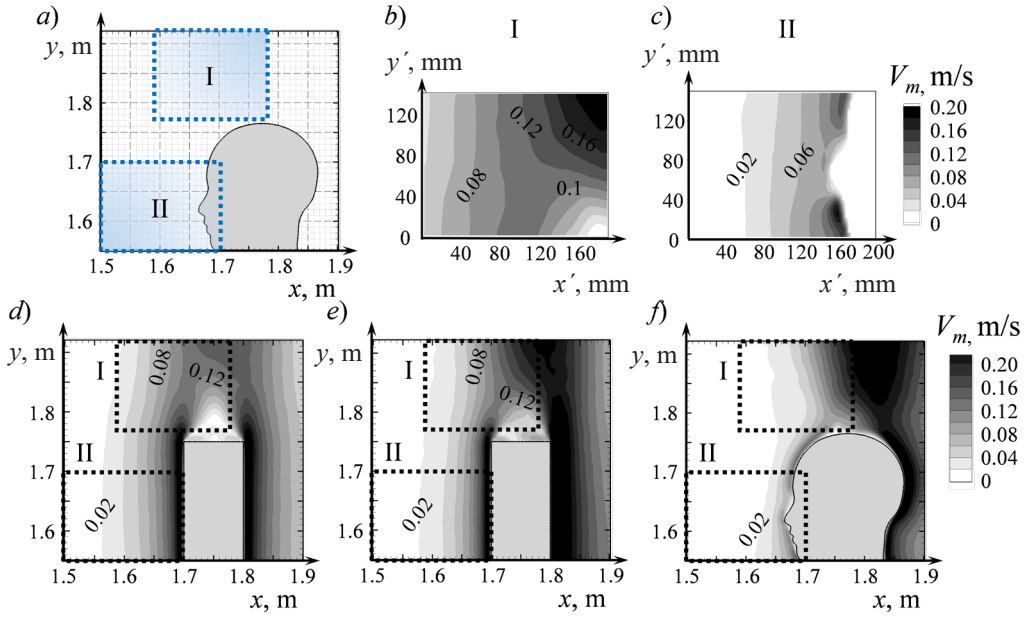

Fig. 7. Layout of sections I and II (*a*); comparison of velocity magnitude distributions in sections I (*b*) and II (*c*) based on the experimental data in [13] with the computational results for three manikin shapes: parallelepiped (*d*), block (*e*), detailed (*f*)
(central plane $z = 1.5$ m is shown)

in [13] for the experimental data given. The velocity fields obtained from the numerical simulation data for the cases with different manikin shapes are shown in Fig. 7,*d*,*e*,*f*. The velocity magnitude is constructed by all three velocity components but the contribution of the velocity component V_z in the central section is minimal.

As the shape of thermal manikin changes, the structure of upward flow near its surface changes considerably: the characteristic values of velocity in front of the manikin (at $x < 1.7$ m) are noticeably higher for the cases with the block and parallelepiped shapes than for the detailed shape. The statement in the case of a simplified (flat) manikin shape, in the absence of any inhomogeneities on the surface, is close to the problem of free-convection flow near a heated plate, where the upward velocity increases upstream. Complex three-dimensional free-convection upward flow evolves near the front of the torso in the case with the detailed manikin shape; this flow changes direction around the manikin's shoulders, and, judging from the streamlines (see Fig. 5,*d*), the air rising near the torso flows over the shoulders to the back of the manikin, subsequently moving upward along the back of the head. Thus, the velocities in the facial region are noticeably lower for a detailed manikin than those obtained for simplified manikins (parallelepiped and block).

Fig. 8 shows the velocity distributions in several sections of the room, obtained in the experiment and through computations for three manikin shapes. Fig. 8,*c* shows the velocity distribution along line l_6 located in section II; the coordinate x' is measured from the surface of the manikin's face. The computed flow structure near the detailed manikin in section II (near the face) agrees with the flow structure obtained in the experiment both qualitatively (see Fig. 7) and quantitatively (Fig. 8,*c*). The velocity values in this region appear to be overestimated by approximately two times for simpler manikin shapes (both block and parallelepiped).

The velocity values in section I can be used to estimate the intensity of the thermal plume emerging above the manikin. The velocity distribution along the line l_5 in this section is shown in Fig. 8,*b*. As noted above, changing the shape of the manikin substantially changes the position of the thermal plume and the characteristic velocities of the upward flow. The data on the velocity in section I

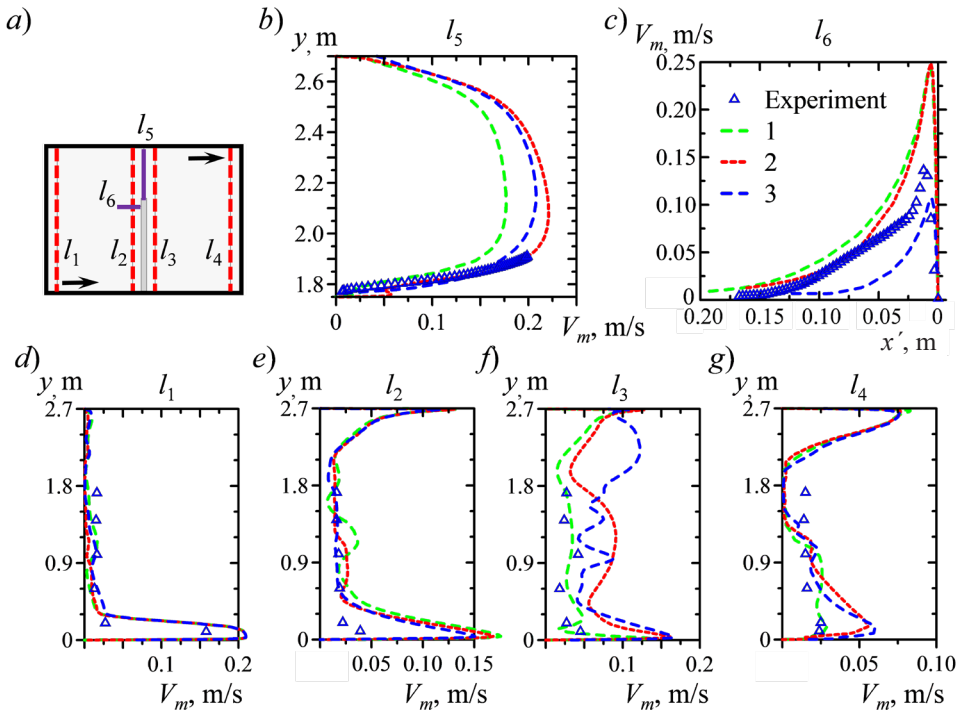

Fig. 8. Layout of the sections (*a*); velocity profiles plotted along the lines $l_1 - l_6$ ($b - g$), obtained in solutions using three manikin shapes:
parallelepiped (*1*), block (*2*) and detailed (*3*)

that are closest to the experiment can be obtained using both the detailed and block shapes of the manikin.

The velocity distributions away from the manikin surface are shown in Fig. 8,*d*,*e*,*g*. Analyzing the graphs, we can see satisfactory agreement between the computational results and experimental data in the region of the near-wall jet (sections l_1 and l_2 at $y < 0.3$ m): however, the computed velocities are somewhat higher than experimental data. The characteristic velocities amount to 0.025 m/s in the region of low-velocity flow in front of manikin (section l_1 at $y > 0.3$ m and l_2 at $0.6 < y < 2.1$ m). Here, the computational data generally agree with the experimental velocities. Changing the shape of the manikin apparently has a rather weak effect on the flow structure in this region.

The shape of the manikin has a more pronounced effect on the flow structure in the section l_3, located directly behind the manikin near the surface (Fig. 8,*f*). The variation range of characteristic velocities does not exceed 0.1 m/s in this region. Experimental velocities are lower than those computed for all manikin shapes. Evidently, the reason for the differences between the computational and experimental data in this region is that the position of the manikin's legs is not reproduced exactly in numerical simulation, even in the case of detailed geometry. At the same time, the computational results related to velocity for three different cases of the manikin shape coincide both with each other and with the experimental data in section l_4 (Fig. 8,*g*). There are some differences in the data in the lower corner of the room with $y < 0.6$ m.

Parameters of heat release from the manikin surface. The temperature distributions T_w over the surface of the thermal manikin obtained for cases with a different manikin shape are shown in Fig. 9,*a*–*c*. The corresponding distributions of dimensionless heat transfer coefficient, the Nusselt number

$$\mathrm{Nu} = q_w l_w / \lambda \left(T_{in} - T_w \right),$$

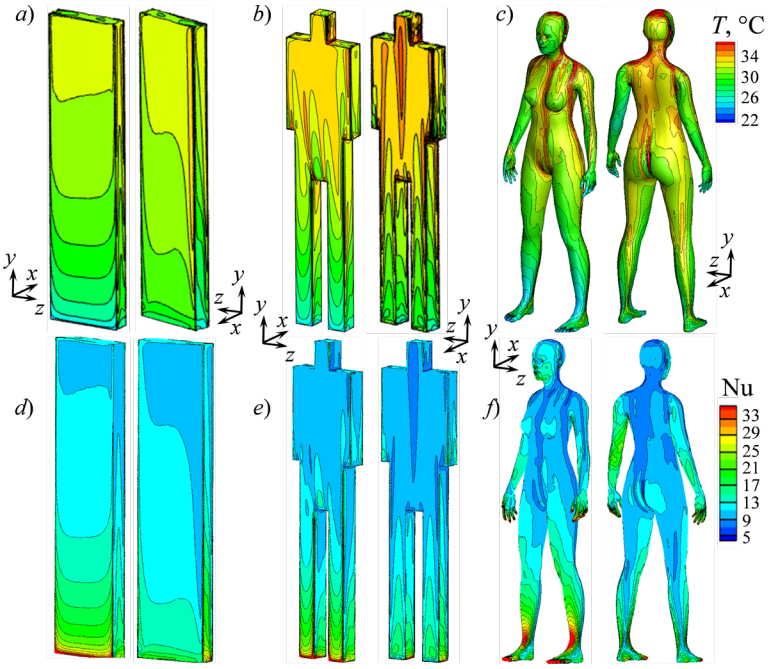

Fig. 9. Computed distributions of temperature ($a - c$) and Nusselt number ($d - f$) over the surfaces of manikins with different shapes: parallelepiped (a, d), block (b, e) and detailed (c, f)

where $l_m = 0.1$ m for all manikin shapes, are shown in Fig. 9,*d*,*e*,*f*.

Table 3 shows the ranges within which the temperature varies over the surfaces of manikins with different shapes: minimum $T_{w,\min}$, maximum $T_{w,\max}$; the temperatures $\langle T_w \rangle$ and Nusselt numbers $\langle \mathrm{Nu} \rangle$ averaged over the manikin surface are also shown.

The temperature distributions for the upwind (opposite to the direction of the x axis) and downwind (along the direction of the x axis) sides differ for all manikin shapes considered. The temperatures are higher from the downwind than from the upwind side; acccordingly, the heat release is lower from this side. There are local differences in temperature distributions for different manikin shapes. In particular, the distribution is almost uniform in the z-direction for the simplest shape (parallelepiped), while a non-uniform distribution is observed for the detailed shape.

Notably, the temperature increases and the heat transfer decreases along the height of the thermal manikin. The minimum temperature on the surface of the manikin is in its lower part. This value is close to the temperature of the inlet air jet $T_{in} = 22$°C, varying slightly from one shape of the manikin to another. The maximum temperature is observed in the upper part of the manikin, near the curved surface. The value $T_{w,\max}$ greatly depends on the shape of the manikin, amounting to 33.6 °C for the parallelepiped, 41.7 °C for the block and 51.4 °C for the detailed shape (see Table 3). The wide variation range of the maximum temperatures corresponding to the detailed shape of the manikin confirms that simplifying the shape of the manikin can produce large errors for the estimated local parameters of thermal comfort. We should note, however, that at such high local temperatures as detected on the surface of the detailed manikin, mechanisms of human body thermoregulation are engaged in the real conditions; neglecting these mechanisms can produce substantially larger uncertainties.

The mean temperature is an integral parameter for the given problem, weakly depending on the geometric shape of the manikin used and amounting to about 31 °C. Importantly, the experimental value of the mean temperature is consistent with the computed one.

Table 3

Comparison of computed and experimental values of parameters related to heat transfer from the surfaces of manikins with different shapes

Parameter	Computed value for			Experiment
	parallelepiped	block	detailed	detailed
$T_{w,\min}$, °C	23.18	23.21	22.33	–
$T_{w,\max}$, °C	33.60	41.70	51.40	–
$\langle T_w \rangle$, °C	30.50	31.30	30.70	32.2
$\langle \mathrm{Nu} \rangle$	13.2	12.1	12.6	10.6

Conclusion

We have carried out a numerical study on the influence that the shape of a heated thermal manikin has on the airflow structure and heat transfer in a model room with displacement ventilation. We have considered three shapes of the manikin: parallelepiped, block and detailed. The computations were
performed based on the RANS approach using the standard k-ε turbulence model.

The sensitivity of the solution to topology and dimension of the computational mesh was examined for the simplest shape, the parallelepiped. It was confirmed that a mesh consisting of polyhedral elements with a dimension of about one million cells, refined near the air jet and the thermal plume, making it possible to obtain a solution that weakly depends on the mesh parameters. We have examined the influence of the dynamic conditions at the inlet on the obtained solution: the flow structure in the vicinity of the manikin was found to be weakly sensitive to the inlet velocity profile in the given velocity range.

The computations indicated that the global flow structure evolving in the room is not symmetrical with respect to the central plane. Two converging solutions were obtained for one of the geometrical configurations, where the jet deflects towards the opposite side walls.

Apparently, the intensity of free-convection airflow was higher in the cases when the detailed and block-type shapes of the manikin were used compared to the configuration with the manikin with the simplest shape, a parallelepiped. Furthermore, the simplification of the manikin shape significantly affects the local characteristics of airflow and heat transfer. On the other hand, the integral parameters only weakly depend on the shape of the manikin used.

As a whole, we can conclude that using a simplified shape of the manikin is reasonable in the cases when it is necessary and does not produce any significant distortion of the solution.

The study was financed by the Russian Foundation for Basic Research, grant no. 20-58-18013.

REFERENCES

1. **Fanger P.O., Melikov A.K., Hanzawa H., Ring J.,** Air turbulence and sensation of draught, Energy and Buildings. 12 (1) (1988) 21–39.

2. ANSI/ASHRAE Standard 62.1–2019. Ventilation for acceptable indoor air quality. 2019. https://www.ashrae.org/technical-resources/bookstore/standards-62-1-62-2

3. **Pei J., Rim D.,** Quality control of computational fluid dynamics (CFD) model of ozone reaction with human surface: Effects of mesh size and turbulence model, Building and Environment. 189 (February) (2021) 107513.

4. **Al Assaad D., Ghali K., Ghaddar N., et al.,** Evaluation of different personalized ventilation air terminal devices: Inhalation vs. clothing-mediated exposures, Building and Environment. 192 (April) (2021) 107637.

5. **Ma J., Qian H., Nielsen P.V., et al.,** What dominates personal exposure? Ambient airflow pattern or local human thermal plume, Building and Environment. 196 (June) (2021) 107790.

6. **Liu J., Zhu S., Kim M.K., Srebric J.,** A review of CFD analysis methods for personalized ventilation (PV) in indoor built environments, Sustainability. 11 (15) (2019) 4166.

7. **Berrouk A.S., Lai A.C.K., Cheung A.C.T., Wong S.L.,** Experimental measurements and large eddy simulation of expiratory droplet dispersion in a mechanically ventilated enclosure with thermal effects, Building and Environment. 45 (2) (2010) 371–379.

8. **Taghinia J.H., Rahman M.M., Lu X.,** Effects of different CFD modeling approaches and simplification of shape on prediction of flow field around manikin, Energy and Buildings. 170 (1 July) (2018) 47–60.

9. **Zukowska D., Melikov A., Popiolek Z.,** Thermal plumes above a simulated sitting person with different complexity of body geometry, Proceedings of Roomvent 2007, The Tenth International Conference on Air Distribution in Rooms, Helsinki, Finland, June 13–15, 3 (2007) 191–198.

10. **Topp C., Hesselholt P., Trier M.R., Nielsen P.V.,** Influence of geometry of thermal manikins on room airflow, Proceedings of ISIAQ 7th International Conference "Healthy Buildings 2003", Singapore, December 7–22, 2003.

11. **Brohus H., Nielsen P.V.,** CFD models of persons evaluated by full-scale wind channel experiments, Proceedings of Roomvent'96, The Fifth International Conference on Air Distribution in Rooms, Yokohama, Japan, July 17–19, 1996. 2 (1996) 137–144.

12. **Yan Y., Li X., Yang L., Tu J.,** Evaluation of manikin simplification methods for CFD simulations in occupied indoor environments, Energy and Buildings. 127 (1 September) (2016) 611–626.

13. **Nielsen P.V., Murakami S., Kato S., et al.,** Benchmark tests for a computer simulated person, Indoor Environmental Engineering, Aalborg University, Aalborg, Denmark, 2003.

14. **Deevy M., Sinai Y., Everitt P., et al.,** Modelling the effect of an occupant on displacement ventilation with computational fluid dynamics, Energy and Buildings. 40 (3) (2008) 255–264.

15. **Martinho N., Lopes A., Silva M.,** CFD modelling of benchmark tests for flow around a detailed computer simulated person, Proceedings of the 7th International Thermal Manikin and Modelling Meeting (at University of Coimbra), September, 2008.

16. **Martinho N., Lopes A., da Silva M.G.,** Evaluation of errors on the CFD computation of air flow and heat transfer around the human body, Building and Environment. 58 (December) (2012) 58–69.

17. **Wilcox D.C.,** Turbulence modeling for CFD, 3-th Ed., DCW Industries, Inc., La Cañada, California, 2006.

18. **Launder B.E., Spalding D.B.,** Lectures in mathematical models of turbulence. Academic Press, London, 1972.

Received 27.06.2021, accepted 20.08.2021.

THE AUTHORS

STEPASHEVA Ekaterina D.
Peter the Great St. Petersburg Polytechnic University
29 Politechnicheskaya St., St. Petersburg, 195251, Russian Federation
momoirin@yandex.ru

ZASIMOVA Marina A.
Peter the Great St. Petersburg Polytechnic University
29 Politechnicheskaya St., St. Petersburg, 195251, Russian Federation
zasimova_ma@spbstu.ru

IVANOV Nikolay G.
Peter the Great St. Petersburg Polytechnic University
29 Politechnicheskaya St., St. Petersburg, 195251, Russian Federation
ivanov_ng@spbstu.ru

СПИСОК ЛИТЕРАТУРЫ

1. **Fanger P.O., Melikov A.K., Hanzawa H., Ring J.** Air turbulence and sensation of draught // Energy and Buildings. 1988. Vol. 12. No. 1. Pp. 21–39.

2. ANSI/ASHRAE Standard 62.1–2019. Ventilation for acceptable indoor air quality. 2019. https://www.ashrae.org/technical-resources/bookstore/standards-62-1-62-2

3. **Pei J., Rim D.** Quality control of computational fluid dynamics (CFD) model of ozone reaction with human surface: Effects of mesh size and turbulence model // Building and Environment. 2021. Vol. 189. February. P. 107513.

4. **Al Assaad D., Ghali K., Ghaddar N., Katramiz E., Ghani S.** Evaluation of different personalized ventilation air terminal devices: Inhalation vs. clothing-mediated exposures // Building and Environment. 2021. Vol. 192. April. P. 107637.

5. **Ma J., Qian H., Nielsen P.V., Liu L., Li Y., Zheng X.** What dominates personal exposure? Ambient airflow pattern or local human thermal plume // Building and Environment. 2021. Vol. 196. June. P. 107790.

6. **Liu J., Zhu S., Kim M.K., Srebric J.** A review of CFD analysis methods for personalized ventilation (PV) in indoor built environments // Sustainability. 2019. Vol. 11. No. 15. P. 4166.

7. **Berrouk A.S., Lai A.C.K., Cheung A.C.T., Wong S.L.** Experimental measurements and large eddy simulation of expiratory droplet dispersion in a mechanically ventilated enclosure with thermal effects // Building and Environment. 2010. Vol. 45. No. 2. Pp. 371–379.

8. **Taghinia J.H., Rahman M.M., Lu X.** Effects of different CFD modeling approaches and simplification of shape on prediction of flow field around manikin // Energy and Buildings. 2018. Vol. 170. 1 July. Pp. 47–60.

9. **Zukowska D., Melikov A., Popiolek Z.** Thermal plumes above a simulated sitting person with different complexity of body geometry // Proceedings of Roomvent 2007, The Tenth International Conference on Air Distribution in Rooms. Helsinki, Finland, June 13–15, 2007. Vol. 3. Pp. 191–198.

10. **Topp C., Hesselholt P., Trier M.R., Nielsen P.V.** Influence of geometry of thermal manikins on room airflow // Proceedings of ISIAQ 7th International Conference "Healthy Buildings 2003". Singapore, December 7–22, 2003. 6 p.

11. **Brohus H., Nielsen P.V.** CFD models of persons evaluated by full-scale wind channel experiments // Proceedings of Roomvent'96, The Fifth International Conference on Air Distribution in Rooms. Yokohama, Japan, July 17–19, 1996. Vol. 2. Pp. 137–144.

12. **Yan Y., Li X., Yang L., Tu J.** Evaluation of manikin simplification methods for CFD simulations in occupied indoor environments // Energy and Buildings. 2016. Vol. 127. 1 September. Pp. 611–626.

13. **Nielsen P.V., Murakami S., Kato S., Topp C., Yang J.-H.** Benchmark tests for a computer simulated person. Aalborg, Denmark: Indoor Environmental Engineering, Aalborg University, 2003. 7 p.

14. **Deevy M., Sinai Y., Everitt P., Voigt L., Gobeau N.** Modelling the effect of an occupant on displacement ventilation with computational fluid dynamics // Energy and Buildings. 2008. Vol. 40. No. 3. Pp. 255–264.

15. **Martinho N., Lopes A., Silva M.** CFD modelling of benchmark tests for flow around a detailed computer simulated person // Proceedings of the 7th International Thermal Manikin and Modelling Meeting (at University of Coimbra). September, 2008. 6 p.

16. **Martinho N., Lopes A., da Silva M.G.** Evaluation of errors on the CFD computation of air flow and heat transfer around the human body // Building and Environment. 2012. Vol. 58. December. Pp. 58–69.

17. **Wilcox D.C.** Turbulence modeling for CFD. 3-th Ed. La Cañada, California: DCW Industries, Inc., 2006. 515 p.

18. **Launder B.E., Spalding D.B.** Lectures in mathematical models of turbulence. London: Academic Press, 1972. 169 p.

Статья поступила в редакцию 27.06.2021, принята к публикации 20.08.2021.

СВЕДЕНИЯ ОБ АВТОРАХ

СТЕПАШЕВА Екатерина Дмитриевна – *студентка Физико-механического института Санкт-Петербургского политехнического университета Петра Великого, Санкт-Петербург, Российская Федерация.*

195251, Российская Федерация, г. Санкт-Петербург, Политехническая ул., 29

momoirin@yandex.ru

ЗАСИМОВА Марина Александровна – *кандидат физико-математических наук, ассистент Высшей школы прикладной математики и вычислительной физики Санкт-Петербургского политехнического университета Петра Великого, Санкт-Петербург, Российская Федерация.*

195251, Российская Федерация, г. Санкт-Петербург, Политехническая ул., 29

zasimova_ma@spbstu.ru

ИВАНОВ Николай Георгиевич – *кандидат физико-математических наук, доцент Высшей школы прикладной математики и вычислительной физики, заведующий научно-исследовательской лабораторией гидроаэродинамики Санкт-Петербургского политехнического университета Петра Великого, Санкт-Петербург, Российская Федерация.*

195251, Российская Федерация, г. Санкт-Петербург, Политехническая ул., 29

ivanov_ng@spbstu.ru